JOURNAL OF AIRCRAFT
Vol. 31, No. 6, November–December 1994

Postinstability Behavior of a Two-Dimensional Airfoil with a Structural Nonlinearity

S. J. Price*
McGill University, Montreal H3A 2K6, Quebec, Canada
B. H. K. Lee†
National Research Council, Ottawa K1A 0R6, Ontario, Canada
and
H. Alighanbari‡
McGill University, Montreal H3A 2K6, Quebec, Canada

A two-dimensional airfoil with a free-play nonlinearity in pitch subject to incompressible flow has been analyzed. The aerodynamic forces on the airfoil were evaluated using Wagner's function and the resulting equations integrated numerically to give time histories of the airfoil motion. Regions of limit cycle oscillation are detected for velocities well below the linear flutter boundary, and the existence of these regions is strongly dependent on the initial conditions and properties of the airfoil. Furthermore, for small structural preloads, narrow regions of chaotic motion are obtained, as suggested by power spectral densities, phase-plane plots, and Poincaré sections of the airfoil time histories. The existence of this chaotic motion is strongly dependent on a number of airfoil parameters, including, mass, frequency ratio, structural damping, and preload.

Nomenclature

b = semichord
c_h, c_α = linear viscous damping coefficients in heave and pitch
h = heave displacement of the airfoil
I_α = moment of inertia about the elastic axis
k_h, k_α = linear structural stiffness in heave and pitch
M = $\bar{M}/k_\alpha$
$\bar{M}$ = nonlinear structural restoring moment
M_0 = restoring moment at the start of the free-play, see Fig. 2
m = airfoil mass
P = aerodynamic force in the heave direction
p = nondimensional P, Pb/V^2I_α
R = aerodynamic pitching moment
r = nondimensional R, Rb^2/V^2I_α
r_α = radius of gyration, $(I_\alpha/mb^2)^{1/2}$
S = airfoil static moment about the elastic axis
U = nondimensional velocity, $V/b\omega_\alpha$
U^* = nondimensional linear flutter velocity
V = freestream velocity
x_α = nondimensional distance from elastic axis to centre of mass, S/mb
α = pitch rotation of the airfoil
$\tilde{\alpha}$ = interpolated estimate of α, see Eqs. (12) and (13)
α_f = α at the start of the free-play, see Fig. 2
δ = free-play angle, see Fig. 2
ζ_h, ζ_α = viscous damping ratios in heave and pitch, $c_h/2m\omega_h$, $c_\alpha/2m\omega_\alpha$
μ = airfoil/air mass ratio, $m/\pi\rho b^2$
ξ = nondimensional heave displacement h/b
τ = nondimensional time, tV/b
ϕ = Wagner's function
ω_h, ω_α = radian frequencies in heave and pitch, $(k_h/m)^{1/2}$, $(k_\alpha/I_\alpha)^{1/2}$
$\bar{\omega}$ = frequency ratio, ω_h/ω_α

Received March 30, 1993; presented as Paper 93-1474 at the AIAA/ASME/ASCE/AHS/ASC 34th Structures, Structural Dynamics, and Materials Conference, La Jolla, CA, April 19–21, 1993; revision received Feb. 11, 1994; accepted for publication Feb. 11, 1994.

*Associate Professor, Department of Mechanical Engineering. Member AIAA.
†Senior Research Officer, High Speed Aerodynamics Laboratory, Institute for Aerospace Research. Associate Fellow AIAA.
‡Graduate Student, Department of Mechanical Engineering.

Introduction

ALTHOUGH the assumptions of linear aerodynamics and structural dynamics are often employed in the aeroelastic analyses of aircraft, there are many examples where nonlinearities exist that can have a significant effect on the aeroelastic response. An excellent review of some possible structural nonlinearities and their effect on aeroelastically induced vibrations is given by Brietbach,[1] and both structural and aerodynamic nonlinearities are considered by Dowell and Ilgamov.[2]

Structural nonlinearities may be classified as being either distributed or concentrated. In general, distributed structural nonlinearities only become appreciable for large amplitude vibrations, whereas concentrated nonlinearities can have a significant effect even for small vibrational amplitudes. One particular concentrated nonlinearity that has received considerable attention in the literature is the bilinear or free-play spring, which is representative of, amongst other possibilities, worn or loose control surface hinges. This can lead to limit cycle oscillations (LCOs) for airspeeds well below the flutter speed predicted based on a linear stiffness, an example of such an LCO for the CF-18 aircraft is discussed by Lee and Tron.[3]

A free-play nonlinearity in pitch was first considered by Woolston et al.[4] Their results, both theoretical (using an analog simulation) and experimental, showed that, depending on the initial pitch displacement, an LCO can occur for velocities significantly less than the linear flutter velocity. Furthermore, at a fixed airspeed the LCO could change from being "mild" to "violent" as the initial pitch displacement was increased. Shen[5] reanalyzed the same problem using a "harmonic balance" or describing function method, this is essentially the first approximation of Krylov and Bogoliubov,[6] and obtained virtually the same results. However, Shen also

demonstrated that significantly different stability boundaries were obtained depending on the amount of preload.

McIntosh et al.[7] analyzed a two-degree-of-freedom airfoil with bilinear structural restraints in both the pitch and heave directions. Theoretical results were obtained via numerical simulations of the time histories, with the aerodynamic forces being predicted from an approximation to Wagner's function. Theory and experiment were found to agree very well in terms of both the airspeed and frequency at the stability boundaries, also LCOs were obtained from both the experimental and theoretical results. In addition, in at least one case, the behavior of the airfoil was shown to be extremely dependent on the initial pitch deflection—for small deflections an LCO was obtained, while for larger deflections a divergent flutter occurred.

Yang and Zhao[8] also considered a two-dimensional airfoil in incompressible flow. Theoretical results were obtained using both digital simulation in the Laplace domain and harmonic balance methods, although in both cases the aerodynamics were obtained using Theodorsen's function, which is strictly correct for harmonic motion only. With a bilinear structural restraint in pitch, LCOs were obtained for airspeeds well below the linear flutter boundary; the amplitude of oscillation increasing as the airspeed increased. Experimentally it was found that with a structural free-play in the pitch direction, LCOs were also obtained for airspeeds below the linear flutter speed, and for some airspeeds two stable LCOs of different amplitudes were detected; one mild LCO, dominated by pitch motion, and a second more violent LCO with both a higher frequency and amplitude than the milder one, and dominated by heave motion. Unfortunately, Yang and Zhao do not distinguish the velocity regions where one or two LCOs occurred, or the difference in initial conditions which led to the different LCOs.

Hauenstein et al.[9,10] considered experimentally and theoretically a rigid wing flexibility mounted at its root with free-play nonlinearities in both the pitch and heave directions. In the theoretical analysis the aerodynamic forces were predicted using an unsteady subsonic doublet lattice technique, and the resulting equations integrated numerically. Experimentally, time histories of both the pitch and heave displacements were measured. An excellent agreement between theory and experiment, in terms of time histories, and their spectral and phase-plane plots, is given by Hauenstein et al. for one specific case with free-play nonlinearities in both the pitch and heave directions. Experimentally, divergent flutter was obtained at an airspeed of 60 ft/s. However, a significant aeroelastic response occurred at an airspeed as low as 35 ft/s; based on the nonrepeatability of the phase-plane plot and the broadness of the frequency spectra, Hauenstein et al. concluded that this motion was chaotic. As the airspeed was further increased, the aeroelastic response became more orderly, with a single-frequency LCO occurring at 50 ft/s. However, based on results not presented, Hauenstein et al. conclude that chaotic motion is not obtainable with a single root nonlinearity. Furthermore, they state that the range of chaotic motion is very dependent on the magnitude of the free-play region.

Recently, Tang and Dowell[11] analyzed the combined flap-pitch motion of a helicopter blade wind-tunnel model with no rotation. The general analysis accounted for both a structural free-play nonlinearity in pitch, and aerodynamic stall using the ONERA model.[12] However, the two simpler cases accounting for either one of the two nonlinearities individually were solved first. With the nonlinear structural model, LCOs were obtained for velocities below the linear flutter boundary. Furthermore, the harmonic balance method showed that for a narrow range of velocities, two LCOs with different amplitudes could exist. Numerical integration of the equations showed the possibility of chaos in this velocity range. Chaos was also obtained for forced oscillations of the blade accounting for the nonlinear aerodynamics with a linear structural model, although only for a narrow range of parameters. Considering the forced oscillation of a blade with both the nonlinear aerodynamics and free-play, it was shown that at a particular velocity the blade response could be either periodic, chaotic, or divergent—depending on the initial conditions. In particular, the type of motion was very sensitive to the initial conditions of the flapping motion.

In this article a further analysis is presented for a two-dimensional airfoil subject to incompressible flow with a structural free-play nonlinearity in pitch. The resulting equations are analyzed using a finite difference technique with the particular aim of examining the sensitivity of the airfoil aeroelastic response to its initial conditions. Phase-plane maps, Poincaré sections, bifurcation diagrams, and spectral analysis are used to investigate the possibility of chaotic behavior. Contrary to previous published results,[10] chaotic motion can exist for a single structural nonlinearity in the pitch motion. However, chaos is detected only for specific airfoil parameters and is confined to small regions in the stability boundary diagram.

Theoretical Analysis

The analysis presented in this article is very similar to that given by Lee and Desrochers,[13] and thus, only the most pertinent details are given. Considering the two-dimensional airfoil, shown schematically in Fig. 1, its equations of motion about the elastic axis may easily be obtained, e.g., Fung,[14] and are given by

$$m\ddot{h}(t) + S\ddot{\alpha}(t) + c_h\dot{h}(t) + k_h h(t) = P(t) \tag{1}$$

$$S\ddot{h}(t) + I_\alpha\ddot{\alpha}(t) + c_\alpha\dot{\alpha}(t) + \bar{M}(\alpha) = R(t) \tag{2}$$

where $\bar{M}$ represents the nonlinear structural restoring moment in the pitch direction. If the structure were linear then $\bar{M}$ would simply be replaced by $k_\alpha\alpha$. These equations may more conveniently be written in nondimensional form, giving

$$\xi''(\tau) + x_\alpha\alpha''(\tau) + (2\zeta_\xi\bar{\omega}/U)\xi'(\tau) + (\bar{\omega}/U)^2\xi(\tau) = p(\tau) \tag{3}$$

$$(x_\alpha/r_\alpha^2)\xi''(\tau) + \alpha''(\tau) + (2\zeta_\alpha/U)\alpha'(\tau) + M(\alpha)/U^2 = r(\tau) \tag{4}$$

where $p(\tau)$ and $r(\tau)$ are the nondimensional force and moment, respectively; M is the structural nonlinearity normalized with respect to the linear torsional stiffness $\bar{M}/k_\alpha$, $\bar{\omega}$ is the frequency ratio ω_ξ/ω_α, and U is the nondimensional airspeed $V/b\omega_\alpha$.

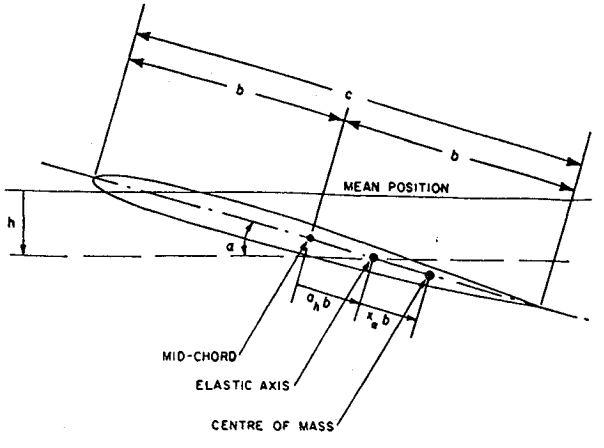

Fig. 1 Schematic representation of the two-degree-of-freedom airfoil.

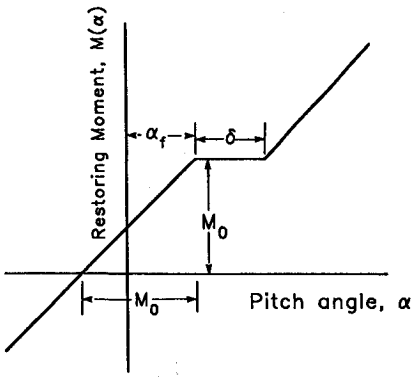

Fig. 2 Structural nonlinearity in the pitch sense.

For incompressible flow $p(\tau)$ and $r(\tau)$ may be obtained (see, e.g., Fung[14]) for any arbitrary motion in terms of the airfoil initial conditions and Wagner's function, $\phi(\tau)$, giving

$$p(\tau) = \frac{-1}{\mu}[\xi''(\tau) - a_h\alpha''(\tau) + \alpha'(\tau)] \times \frac{-2}{\mu}\left\{[\alpha(0) + \xi'(0) + \overline{a_h}\alpha'(0)]\phi(\tau) + \int_0^\tau \phi(\tau - \sigma)[\alpha'(\sigma) + \xi''(\sigma) + \overline{a_h}\alpha''(\sigma)]\, d\sigma\right\} \quad (5)$$

$$r(\tau) = \frac{2}{\mu r_\alpha^2}\left(\frac{1}{2} + a_h\right)\left\{[\alpha(0) + \xi'(0) + \overline{a_h}\alpha'(0)]\phi(\tau) + \int_0^\tau \phi(\tau - \sigma)[\alpha'(\sigma) + \xi''(\sigma) + \overline{a_h}\alpha''(\sigma)]\, d\sigma\right\} + \frac{1}{\mu r_\alpha^2}\left\{a_h[\xi''(\tau) - a_h\alpha''(\tau)] - \overline{a_h}\alpha'(\tau) - \frac{1}{8}\alpha''(\tau)\right\} \quad (6)$$

where $\overline{a_h} = (\frac{1}{2} - a_h)$, $\phi(\tau) = 1 - ae^{-b\tau} - ce^{-d\tau}$, $l = 1$, $a = 0.165$, $b = 0.0455$, $c = 0.335$, and $d = 0.3$.

The specific structural nonlinearity considered in this article is a free-play in the pitch direction with preload, and is shown schematically in Fig. 2. Using the notation given in Fig. 2, $M(\alpha)$ is given by

$$M(\alpha) = \begin{cases} \alpha - \alpha_f + M_0 & \text{for } \alpha < a_f \\ M_0 & \text{for } \alpha_f \le \alpha \le \alpha_f + \delta \\ \alpha - \alpha_f - \delta + M_0 & \text{for } \alpha_f + \delta < \alpha \end{cases} \quad (7)$$

To solve the above equations, Houbolt's finite difference method[15] is employed. This has been shown to be more efficient than higher order finite difference schemes, yet still have good accuracy.[16] The derivatives at time $\tau + \Delta\tau$ are replaced by backward difference formulas using values at three previous times. For example

$$\alpha''(\tau + \Delta\tau) = [2\alpha(\tau + \Delta\tau) - 5\alpha(\tau) + 4\alpha(\tau - \Delta\tau) - \alpha(\tau - 2\Delta\tau)]/\Delta\tau^2 \quad (8)$$

$$\alpha'(\tau + \Delta\tau) = [11\alpha(\tau + \Delta\tau) - 18\alpha(\tau) + 9\alpha(\tau - \Delta\tau) - 2\alpha(\tau - 2\Delta\tau)]/6\Delta\tau \quad (9)$$

and similarly for $\xi''(\tau + \Delta\tau)$ and $\xi'(\tau + \Delta\tau)$. Hence, in difference form, Eqs. (3) and (4) can be expressed, after considerable algebra, as

$$\bar{P}_{11}\alpha(\tau + \Delta\tau) + \bar{P}_{12}\xi(\tau + \Delta\tau) = \bar{X}_1 \quad (10)$$

$$[\bar{P}_{21} + U^{-2}M_p]\alpha(\tau + \Delta\tau) + \bar{P}_{22}\xi(\tau + \Delta\tau) = \bar{X}_2 - M_\alpha/U^2 \quad (11)$$

In Eq. (11) $M(\alpha)$ has been replaced by $M_p\alpha(\tau + \Delta\tau) + M_\alpha$, where

$$M_p = \begin{cases} 1 & \text{for } \bar{\alpha} < \alpha_f \text{ and } \alpha_f + \delta < \bar{\alpha} \\ 0 & \text{otherwise} \end{cases} \quad (12)$$

M_α is given by

$$M_\alpha = \begin{cases} M_0 - \alpha_f & \text{for } \bar{\alpha} < \alpha_f \\ M_0 & \text{for } \alpha_f \le \bar{\alpha} \le \alpha_f + \delta \\ M_0 - \alpha_f - \delta & \text{for } \alpha_f + \delta < \bar{\alpha} \end{cases} \quad (13)$$

and $\bar{\alpha}$ is an estimate of α that is obtained by linear extrapolation from τ to $\tau + \Delta\tau$. The terms $\bar{P}_{11}$, $\bar{P}_{12}$, $\bar{P}_{21}$, $\bar{P}_{22}$, $\bar{X}_1$, and $\bar{X}_2$ are given in the Appendix. Solution of the above equation yields the values of α and ξ at time $\tau + \Delta\tau$.

As shown in Eqs. (5) and (6), the aerodynamic forces and moments depend upon terms that include $\int_0^\tau \phi(\tau - \sigma)\, d\sigma$, these were evaluated numerically using Simpson's rule. This numerical integration is automatically evaluated via the $\bar{P}$ and $\bar{X}$ expressions given in the Appendix.

Houbolt's finite difference scheme requires values of α and ξ at times $\tau - 2\Delta\tau$, $\tau - \Delta\tau$, and τ in order to determine the respective values at $\tau + \Delta\tau$. Hence, at time $\tau = 0$, a starting procedure is required to give the values of α and ξ at times $\tau - 2\Delta\tau$ and $\tau - \Delta\tau$; this is outlined below.

Using Taylor's series the following can be written:

$$\alpha(-\Delta\tau) = \alpha(0) - \Delta\tau\alpha'(0) + \Delta\tau^2/2\alpha''(0) + \mathcal{O}(\Delta\tau^3) \quad (14)$$

and similarly for α', α'', and ξ. Hence, given the initial conditions and Eq. (14), appropriate values of α and ξ at $-2\Delta\tau$ and $-\Delta\tau$ can be evaluated.

Results and Discussion

Numerical simulations of the airfoil heave and pitching response have been obtained for a number of different combinations of the following parameters: amount of free-play, δ; preload, α_f and M_0; initial conditions of the airfoil, $\alpha(0)$, $\alpha'(0)$, $\xi(0)$, and $\xi'(0)$; frequency ratio, $\bar{\omega} = \omega_\xi/\omega_\alpha$; $\mu = m/\pi\rho b^2$; and structural damping, ζ_α and ζ_ξ. Only a sample of the results obtained will be presented here, and all are for zero structural damping.

U^* was first obtained by removing the free-play and then increasing U until divergent oscillations of α and ξ were obtained. This was also checked using a standard U-g analysis, which to some extent verified the numerical finite difference method employed in the nonlinear calculations. In all cases the air speed U is presented, normalized with respect to U^*.

Results with a Preload

Detailed simulations were first done for the following set of parameters: $\bar{\omega} = 0.2$, $\mu = 100$, $\alpha_f = 0.25$ deg, $\delta = 0.5$ deg, and $M_0 = 0.25$ deg; note, as shown in Fig. 2, because of the manner in which the structural nonlinearity has been normalized, M_0 has the same units as α or δ. As U was increased for a fixed $\alpha(0)$, with $\alpha'(0) = \xi(0) = \xi'(0) = 0$ convergent stable motion was followed by LCOs and then divergent flutter at $U = U^*$. However, for some values of $\alpha(0)$, as U was increased, LCOs were followed by stable motion, then LCOs again, and finally divergent flutter. For example, at $\alpha(0) = 7.5$ deg, the results in Fig. 3 show time histories of the pitch displacement during the first set of LCOs, during the intermediate stable region, and finally during the second set of LCOs.

Similar time histories were computed for a wide range of $\alpha(0)$ and a map showing the types of airfoil motion is presented in Fig. 4. As shown, "islands" of LCOs exist for U below the main boundary of LCOs—only the main islands of LCOs are shown in Fig. 4, in addition, some very small regions of LCO motion were observed between the islands

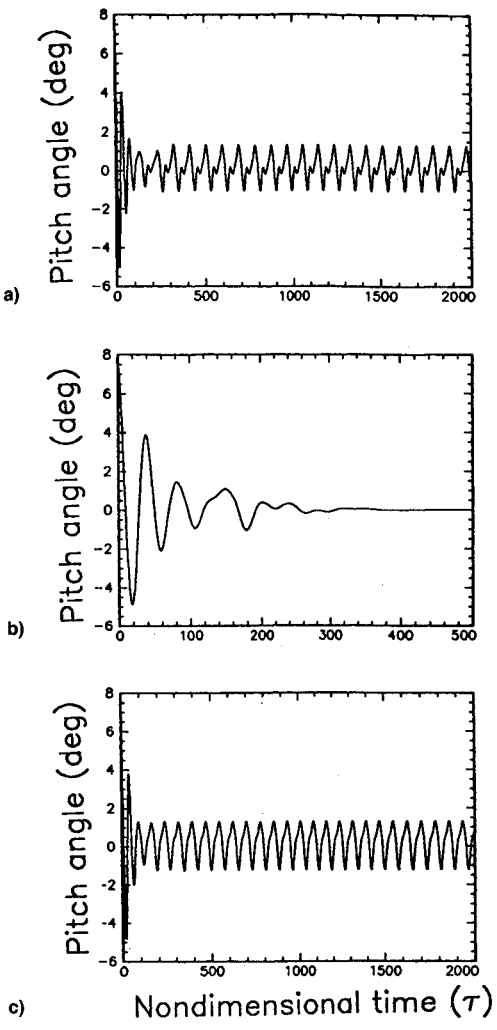

Fig. 3 Time history of pitch angle of the airfoil, $\bar{\omega} = 0.2$, $\mu = 100$, $\alpha_f = 0.25$ deg, $\delta = 0.5$ deg, $M_0 = 0.25$ deg, $\alpha(0) = 7.5$ deg, $\alpha'(0) = \xi(0) = \xi'(0) = 0$: a) $U/U^* = 0.763$, b) $U/U^* = 0.80$, and c) $U/U^* = 0.826$.

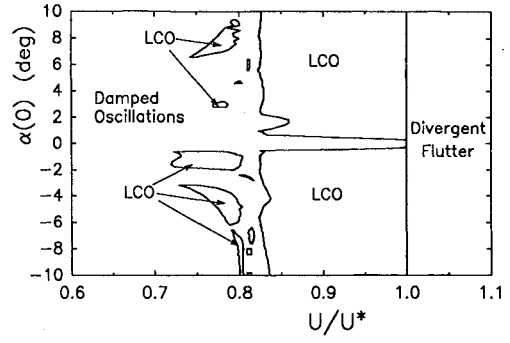

Fig. 4 Stability boundary for the airfoil as a function of initial pitch rotation, $\bar{\omega} = 0.2$, $\mu = 100$, $\alpha_f = 0.25$ deg, $\delta = 0.5$ deg, $M_0 = 0.25$ deg, $\alpha'(0) = \xi(0) = \xi'(0) = 0$.

and the main boundary of LCO motion. The existence of these islands was very dependent on the free-play and preload conditions, e.g., with $M_0 = \alpha_0 = \delta = 0.5$ deg no islands were obtained.

Power spectral densities (PSDs) of the time traces were also obtained, and typical examples are shown in Fig. 5. In Fig. 5a the pitching motion in one of the LCO islands, at $U/U^* = 0.79$, is presented, the motion is dominated by two frequencies at $0.335\omega_\alpha$ and $0.67\omega_\alpha$—although there are a number of other very distinct frequency peaks in the spectrum, their amplitudes are small compared to the fundamental and first

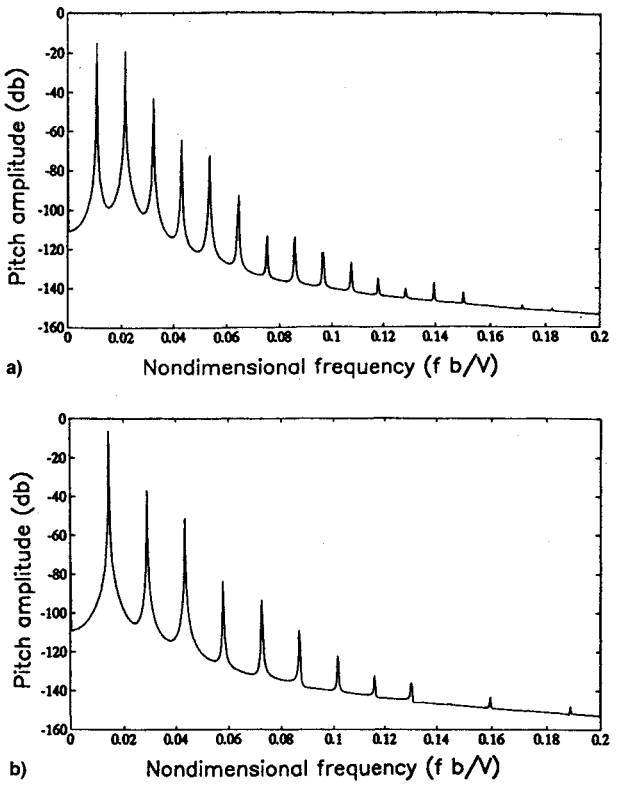

Fig. 5 Power spectral densities of the pitch rotation of the airfoil, $\bar{\omega} = 0.2$, $\mu = 100$, $\alpha_f = 0.25$ deg, $\delta = 0.5$ deg, $M_0 = 0.25$ deg, $\alpha_0 = 7.5$ deg: a) $U/U^* = 0.79$ and b) $U/U^* = 0.85$.

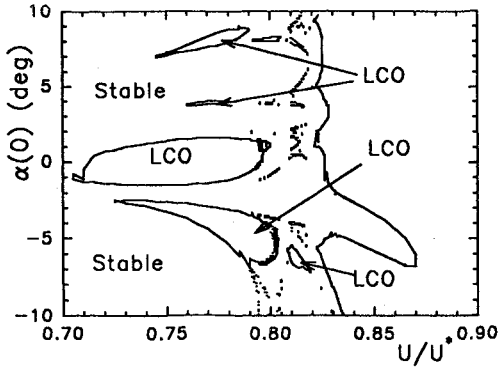

Fig. 6 Stability boundary for the airfoil as a function of initial pitch rotation, $\bar{\omega} = 0.2$, $\mu = 100$, $\alpha_f = 0.25$ deg, $\delta = 0.5$ deg, $M_0 = 0.25$ deg, $\alpha'(0) = 0.229b/V$ deg/s, $\xi(0) = \xi'(0) = 0$.

harmonic. The heave motion (not shown) has one significant peak only, at a frequency of $0.34\omega_\alpha$. In the main region of the LCO motion both the pitch and heave motion have only one dominant frequency, e.g., at $U/U^* = 0.85$ both the heave and pitching motion frequencies are 0.48 ω_α, see Fig. 5b for the pitch motion.

At first the existence of these islands of LCO motion was a little perplexing, and indeed there was some concern over whether these islands really existed or whether they were due to convergence not being achieved in the numerical integration. However, some very long time integrations confirmed the existence of these islands. Furthermore, their origin becomes more apparent when it is realized that Fig. 4 represents only a two-dimensional section through the five-dimensional boundary between stable oscillations and LCO motions; the five dimensions being U, $\alpha(0)$, $\alpha'(0)$, $\xi(0)$, and $\xi'(0)$. A similar two-dimensional section to that shown in Fig. 4 but, with $\alpha'(0) = 0.229b/V$ deg/s is shown in Fig. 6. Once again islands of LCO motion are obtained below the main LCO boundary, but the shape of both these islands and the main boundary

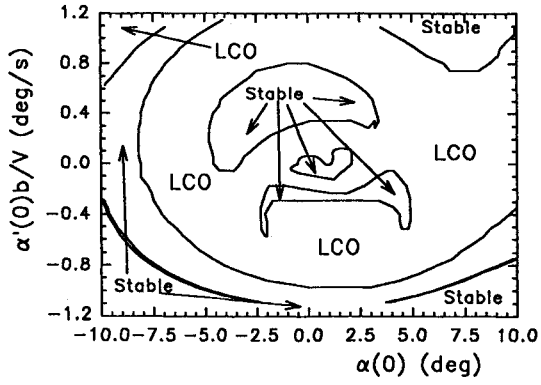

Fig. 7 Stability boundary for the airfoil as a function of $\alpha(0)$ and $\alpha'(0)$ for constant velocity, $\bar{\omega} = 0.2$, $\mu = 100$, $\alpha_f = 0.25$ deg, $\delta = 0.5$ deg, $M_0 = 0.25$ deg, $\xi(0) = \xi'(0) = 0$, $U/U^* = 0.83$.

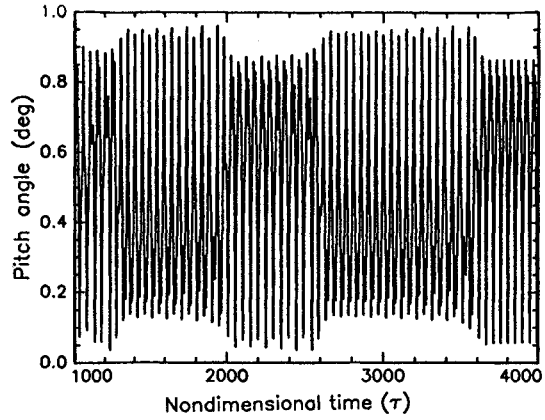

Fig. 8 Time history of airfoil pitch motion, $U/U^* = 0.3$, $\bar{\omega} = 0.2$, $\mu = 100$, $\alpha_f = 0.25$ deg, $\delta = 0.5$ deg, $M_0 = 0.0$ deg, $\alpha(0) = 7.0$ deg, $\alpha'(0) = \xi(0) = \xi'(0) = 0$.

are very different to that shown in Fig. 4. One common feature between the results of Figs. 4 and 6 (and many others not shown here) is the multitude of small islands of LCO motion for $0.79 \leq U/U^* \leq 0.84$, approximately. The reason for the large number of these small islands can be seen if a different two-dimensional section through the five-dimensional boundary is taken, showing the stability boundary as a function of $\alpha(0)$ and $\alpha'(0)$ for constant $\xi(0)$, $\xi'(0)$ and U. Such a set of results is presented in Fig. 7 for $U/U^* = 0.83$, showing a very complex boundary between LCO and stable motion. Indeed, based on the totality of results obtained, it can be concluded that the five-dimensional boundary is in fact a continuous geometric shape with a number of protuberances that spiral out from the main body; furthermore, the apparent islands that appear in Figs. 4 and 6 are due to taking two-dimensional sections through this five-dimensional body.

A further significant point to note from the results with preload can be seen from Fig. 4. The equilibrium position ($\alpha = \xi = 0.0$) is stable for all values of $U \leq U^*$; hence, the instability at $U = U^*$ is, using the terminology of nonlinear dynamics, a subcritical Hopf bifurcation. Hence, it is apparent that for $U \leq U^*$, there must also be an unstable limit cycle between the stable focus and the stable limit cycle.

Results with No Preload

A second example for which extensive numerical simulations were done was for $\bar{\omega} = 0.2$, $\mu = 100$, $\alpha_f = 0.25$ deg, $\delta = 0.5$ deg, and $M_0 = 0.0$ deg; note this differs from the previous example only in the value of M_0. For this set of parameters it was found that for some velocities below the linear flutter speed, no matter how long the simulation was allowed to run, the time histories never reached a steady-state condition; see, e.g., Fig. 8. It was suspected that this may

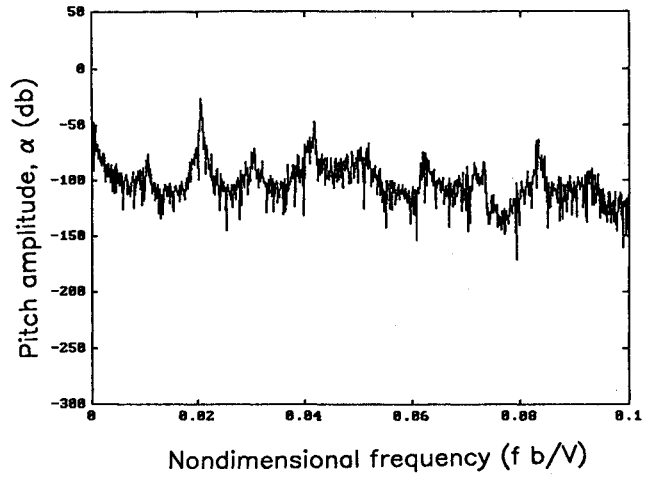

Fig. 9 Power spectral density of the airfoil pitch motion, $U/U^* = 0.3$, $\bar{\omega} = 0.2$, $\mu = 100$, $\alpha_f = 0.25$ deg, $\delta = 0.5$ deg, $M_0 = 0.0$ deg, $\alpha(0) = 7.0$ deg, $\alpha'(0) = \xi(0) = \xi'(0) = 0$.

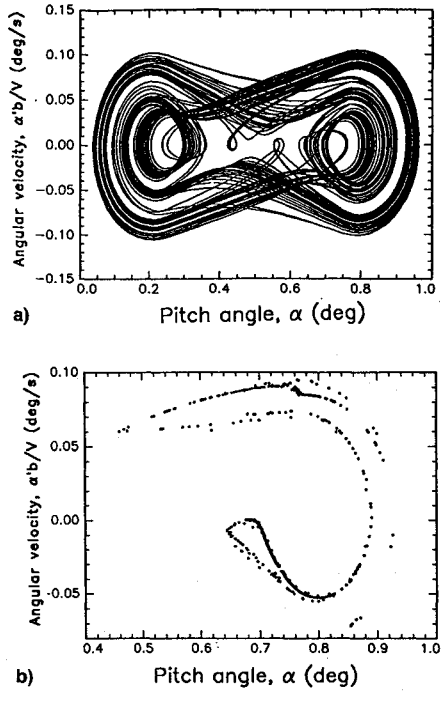

Fig. 10 a) Phase-plane and b) Poincaré section (for $\dot{\xi} = 0$ and $\xi \geq -0.02$); $U/U^* = 0.3$, $\bar{\omega} = 0.2$, $\mu = 100$, $\alpha_f = 0.25$ deg, $\delta = 0.5$ deg, $M_0 = 0.0$ deg, $\alpha(0) = 7.0$ deg, $\alpha'(0) = \xi(0) = \xi'(0) = 0$.

indicate chaos, and this was investigated initially by forming PSDs of the time traces, a typical example of which is shown in Fig. 9. When this PSD is compared with those of Fig. 5 it is clear that it is much more broadband with significantly less dominant frequency peaks; this is typical of chaotic motion.[17]

To add further evidence to the the existence of chaos, phase-plane plots and Poincaré sections were obtained; typical examples of which are shown in Fig. 10, for the data of Figs. 8 and 9. The phase-plane section shown in Fig. 10a is typical of a "two-well potential" and is indicative of chaos. This is very similar to the phase-plane plot obtained by Tang and Dowell[11] for their analysis with a free-play nonlinearity. The Poincaré section shown in Fig. 10b has a very distinct structure that lends further evidence to the existence of chaotic motion; this is in contrast to the results of Tang and Dowell where the Poincaré section was fairly random and showed no distinct structure. Although the results presented in this section cannot be said to conclusively prove the motion to be chaotic, the time histories, PSDs, phase-plane section, and Poincaré

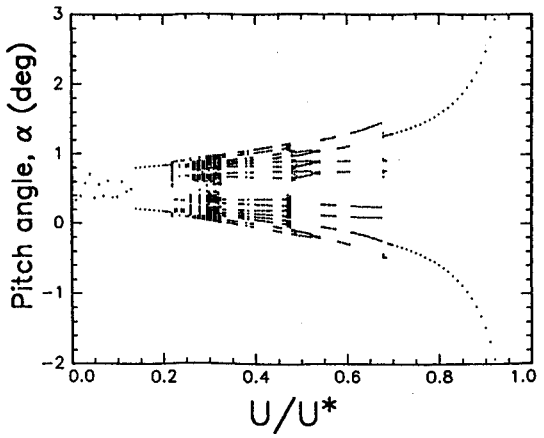

Fig. 11 Bifurcation diagram showing α for $\alpha' = 0$; $\bar{\omega} = 0.2$, $\mu = 100$, $\alpha_f = 0.25$ deg, $\delta = 0.5$ deg, $M_0 = 0.0$ deg, $\alpha(0) = 7.0$ deg, $\alpha'(0) = \xi(0) = \xi'(0) = 0$.

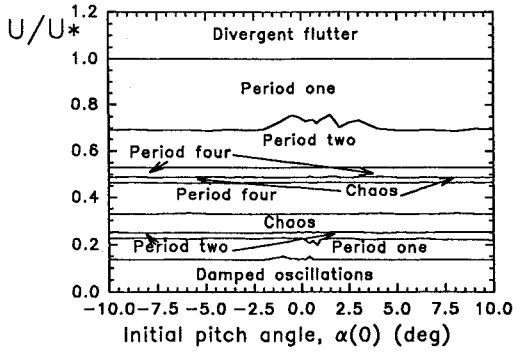

Fig. 12 Approximate stability boundaries for the airfoil as a function of initial pitch rotation, $\bar{\omega} = 0.2$, $\mu = 100$, $\alpha_f = 0.25$ deg, $\delta = 0.5$ deg, $M_0 = 0.0$ deg.

sections are all strongly indicative of the existence of chaos, and thus, it is reasonable to conclude that the motion is indeed chaotic. Ideally, the Lyapunov exponents should be calculated to conclusively establish the existence of chaos; however, because of the nonanalytic nature of the free-play nonlinearity there are problems that prevent this from being done with any certainty. However, the authors[18] recently conducted a very similar analysis to that presented here, but for a cubic nonlinearity. Very similar results were obtained, but because of the analytic nature of the cubic nonlinearity it was possible to determine the complete Lyapunov spectrum, and it was found that one Lyapunov exponent was positive, proving the existence of chaos. Thus, almost certainly the results presented here are also chaotic.

Numerous simulations of the type discussed above were completed, over a wide range of velocities, to determine the range of this chaotic motion; these are best illustrated via a bifurcation diagram as shown in Fig. 11. This diagram shows, as a function of U/U^*, the value of α when $\alpha' = 0$. The significance of the bifurcation diagram is as follows. If at a particular U the system is stable, then a single point is obtained, e.g., $U/U^* \leq 0.13$, approximately. If the motion is an LCO with one frequency, then two points are obtained ($0.14 \leq U/U^* \leq 0.22$, approximately), and an LCO with two frequencies gives four points, etc. However, for some velocities a large number of points are obtained (giving what appears to be almost a vertical line on the bifurcation diagram) indicating chaos; examples of this can be seen in Fig. 11 for $0.29 \leq U/U^* \leq 0.33$, approximately. The bifurcation diagram shown in Fig. 11 suggests that the route to chaos is via "period-doubling." This is much more apparent if the control parameter is taken as $1 - U/U^*$ rather than U/U^*, showing that as velocity is decreased from the divergent flutter boundary there is a large region of period-one motion followed by period-two and period-four motion, and finally chaos.

Using a large number of bifurcation diagrams for different initial values of $\alpha(0)$, a map showing the boundaries of the different types of motion was obtained and is presented in Fig. 12. It is apparent that the initial value of $\alpha(0)$ has much less effect in this case than that obtained with preload, as suggested by Figs. 4 and 6. Unfortunately, the effect of changing $\alpha'(0)$, $\xi(0)$, or $\xi'(0)$ has not been investigated extensively, and thus, it is not possible to say how the regions of chaotic motion are affected by these parameters.

Conclusions

For a two-degree-of-freedom airfoil with a stuctural free-play nonlinearity in pitch, LCOs are obtained for velocities well below the linear flutter boundary. The existence of LCO motion at a particular velocity is strongly dependent on the initial conditions of the airfoil, and the basin of attraction of LCO motion is a very complex five-dimensional shape. If a two-dimensional section is taken through this boundary then it appears that islands of LCOs can exist for velocities below the main boundary of LCO motion. However, these islands are in fact not separate from the main boundary.

Chaotic motion can also exist for velocities below the flutter velocity, although the existence of this chaotic motion is strongly dependent on a number of parameters, specifically preload, frequency ratio, and airfoil/air mass ratio. For example, considering preload, chaos was obtained with $M_0 = \pm 0.05$ deg, but not with $M_0 = 0.25$ deg. Similarly, although chaos was obtained with $\bar{\omega} = 0.2$, it was not obtained with $\bar{\omega} = 0.6$ or 0.667, which could explain why Hauenstein et al.[10] did not obtain chaos with a single nonlinearity in their experiments with a frequency ratio of 0.667. Also, an increase in μ from 100 to 150 significantly increased the velocity range over which chaotic vibrations occurred, while reducing μ to 50 reduced this range. The effect of structural damping on the existence of this chaotic motion has also been investigated, although the results obtained are somewhat contradictory. For example, adding 1% of critical damping in pitch increases the region over which chaotic motion occurs, while adding 1% critical damping in heave reduces the region of chaotic motion.

Appendix: Coefficients in Eqs. (10) and (11)

The coefficients $\bar{P}_{11}$, $\bar{P}_{12}$, $\bar{P}_{21}$, and $\bar{P}_{22}$ in Eqs. (10) and (11) are as follows:

$$\bar{P}_{11} = 2c_2/\Delta\tau^2 + 11c_4/(6\Delta\tau) + c_6$$

$$\bar{P}_{12} = 2c_1/\Delta\tau^2 + 11c_3/(6\Delta\tau) + c_5$$

$$\bar{P}_{21} = 2d_2/\Delta\tau^2 + 11d_4/(6\Delta\tau) + d_6$$

$$\bar{P}_{22} = 2d_1/\Delta\tau^2 + 11d_3/(6\Delta\tau)$$

where the c_i and d_i terms are given by

$$c_1 = 1 + [1 - \tfrac{3}{4}\Delta\tau(a + c)]/\mu$$

$$c_2 = x_\alpha - [a_h + \tfrac{3}{4}\Delta\tau(a + c)\bar{a}_h]/\mu$$

$$c_3 = 2\zeta_\xi\bar{\omega}/U + 2l/\mu$$

$$c_4 = [1 + 2l\bar{a}_h - \tfrac{3}{4}(a + c)\Delta\tau]/\mu$$

$$c_5 = (\bar{\omega}/U)^2$$

$$c_6 = 2l/\mu$$

$$d_1 = [x_\alpha - a_h/\mu + \tfrac{3}{4}\Delta\tau(a + c)(\tfrac{1}{2} + a_h)/\mu]/r_\alpha^2$$

$$d_2 = 1 + [\tfrac{1}{8} + a_h^2 + \tfrac{3}{4}\Delta\tau(a + c)\bar{a}_h(\tfrac{1}{2} + a_h)]/(\mu r_\alpha^2)$$

$$d_3 = -2l(\tfrac{1}{2} - a_h)/(\mu r_\alpha^2)$$

$$d_4 = 2\zeta_\alpha/U + [\bar{a}_h - 2l\bar{a}_h(\tfrac{1}{2} + a_h) + \tfrac{3}{4}\Delta\tau(a + c)(\tfrac{1}{2} + a_h)]/(\mu r_\alpha^2)$$

$$d_6 = -2l(\tfrac{1}{2} + a_h)/(\mu r_\alpha^2)$$

The terms $\bar{X}_1$ and $\bar{X}_2$ in Eqs. (10) and (11) are as follows:

$$\bar{X}_1 = x_{11}\alpha(\tau) + x_{13}\alpha(\tau - \Delta\tau) + x_{15}\alpha(\tau - 2\Delta\tau) + x_{12}\xi(\tau) + x_{14}\xi(\tau - \Delta\tau) + x_{16}\xi(\tau - 2\Delta\tau) + x_{17}$$

$$\bar{X}_2 = x_{21}\alpha(\tau) + x_{23}\alpha(\tau - \Delta\tau) + x_{25}\alpha(\tau - 2\Delta\tau) + x_{22}\xi(\tau) + x_{24}\xi(\tau - \Delta\tau) + x_{26}\xi(\tau - 2\Delta\tau) + x_{27}$$

where the x_{ij} terms are

$$x_{11} = 5c_2/\Delta\tau^2 + 18c_4/(6\Delta\tau)$$

$$x_{12} = 5c_1/\Delta\tau^2 + 18c_3/(6\Delta\tau)$$

$$x_{13} = -4c_2/\Delta\tau^2 - 9c_4/(6\Delta\tau)$$

$$x_{14} = -4c_1/\Delta\tau^2 - 9c_3/(6\Delta\tau)$$

$$x_{15} = c_2/\Delta\tau^2 + 2c_4/(6\Delta\tau)$$

$$x_{16} = c_1/\Delta\tau^2 + 2c_3/(6\Delta\tau)$$

$$x_{17} = 2[L_0 - aI_b(\tau + \Delta\tau) - cI_d(\tau + \Delta\tau) - x_{17a}\lambda(\tau) + x_{17b}\lambda(\tau - \Delta\tau) - x_{17c}\lambda(\tau - 2\Delta\tau)]/\mu$$

$$x_{21} = 5d_2/\Delta\tau^2 + 18d_4/(6\Delta\tau)$$

$$x_{22} = 5d_1/\Delta\tau^2 + 18d_3/(6\Delta\tau)$$

$$x_{23} = -4d_2/\Delta\tau^2 - 9d_4/(6\Delta\tau)$$

$$x_{24} = -4d_1/\Delta\tau^2 - 9d_3/(6\Delta\tau)$$

$$x_{25} = d_2/\Delta\tau^2 + 2d_4/(6\Delta\tau)$$

$$x_{26} = d_1/\Delta\tau^2 + 2d_3/(6\Delta\tau)$$

$$x_{27} = -(\tfrac{1}{2} + a_h)x_{17}/r_\alpha^2$$

where

$$x_{17a} = \tfrac{19}{24}\Delta\tau(ae^{-b\Delta\tau} + ce^{-d\Delta\tau})$$

$$x_{17b} = \tfrac{5}{24}\Delta\tau(ae^{-2b\Delta\tau} + ce^{-2d\Delta\tau})$$

$$x_{17c} = \tfrac{1}{24}\Delta\tau(ae^{-3b\Delta\tau} + ce^{-3d\Delta\tau})$$

$$L_0 = [-ae^{-b(\tau+\Delta\tau)} - ce^{-d(\tau+\Delta\tau)}][\xi'(0) + \bar{a}_h\alpha'(0) + \alpha(0)]$$

$$I_b(\tau + \Delta\tau) = e^{-b\Delta\tau}\{I_b(\tau) + \tfrac{1}{24}\Delta\tau[9\lambda(\tau) + 19\lambda(\tau - \Delta\tau)e^{-b\Delta\tau} - 5\lambda(\tau - 2\Delta\tau)e^{-2b\Delta\tau} + \lambda(\tau - 3\Delta\tau)e^{-3b\Delta\tau}]\}$$

$$I_d(\tau + \Delta\tau) = e^{-d\Delta\tau}\{I_d(\tau) + \tfrac{1}{24}\Delta\tau[9\lambda(\tau) + 19\lambda(\tau - \Delta\tau)e^{-d\Delta\tau} - 5\lambda(\tau - 2\Delta\tau)e^{-2d\Delta\tau} + \lambda(\tau - 3\Delta\tau)e^{-3d\Delta\tau}]\}$$

$$\lambda(\tau) = \xi''(\tau) + \bar{a}_h\alpha''(\tau) + \alpha'(\tau)$$

$$\alpha'(\tau + \Delta\tau) = (1/6\Delta\tau)[11\alpha(\tau + \Delta\tau) - 18\alpha(\tau) + 9\alpha(\tau - \Delta\tau) - 2\alpha(\tau - 2\Delta\tau)]$$

$$\alpha''(\tau + \Delta\tau) = (1/\Delta\tau^2)[2\alpha(\tau + \Delta\tau) - 5\alpha(\tau) + 4\alpha(\tau - \Delta\tau) - \alpha(\tau - 2\Delta\tau)]$$

$$\xi''(\tau + \Delta\tau) = (1/\Delta\tau^2)[2\xi(\tau + \Delta\tau) - 5\xi(\tau) + 4\xi(\tau - \Delta\tau) - \xi(\tau - 2\Delta\tau)]$$

Acknowledgments

The authors gratefully acknowledge the financial support of the Department of National Defence and the Institute for Aerospace Research. The first author also acknowledges the support of the Natural Sciences and Engineering Research Council of Canada.

References

[1]Brietbach, E., "Effect of Structural Nonlinearities on Aircraft Vibration and Flutter," 45th Structures and Materials AGARD Panel Meeting, AGARD Report 665, Voss, Norway, 1977.

[2]Dowell, E. H., and Ilgamov, M., *Studies in Nonlinear Aeroelasticity*, Springer-Verlag, New York, 1988.

[3]Lee, B. H. K., and Tron, A., "Effects of Structural Nonlinearities on Flutter Characteristics of the CF-18 Aircraft," *Journal of Aircraft*, Vol. 26, No. 8, 1989, pp. 781–786.

[4]Woolston, D. S. Runyan, H. L., and Andrews, R. E., "An Investigation of Effects of Certain Types of Structural Nonlinearities on Wing and Control Surface Flutter," *Journal of the Aeronautical Sciences*, Vol. 24, Jan. 1957, pp. 57–63.

[5]Shen, S. F., "An Approximate Analysis of Nonlinear Flutter Problems," *Journal of the Aerospace Sciences*, Vol. 28, Jan. 1959, pp. 25–32, 45.

[6]Krylov, M. N., and Bogoliubov, N. N., *Introduction to Non-Linear Mechanics*, Princeton Univ. Press, Princeton, NJ, 1949.

[7]McIntosh, S. C., Reed, R. E., and Rodden, W. P., "Experimental and Theoretical Study of Nonlinear Flutter," *Journal of Aircraft*, Vol. 18, No. 12, 1981, pp. 1057–1063.

[8]Yang, Z. C., and Zhao, L. C., "Analysis of Limit Cycle Flutter of an Airfoil in Incompressible Flow," *Journal of Sound and Vibration*, Vol. 123, Jan. 1988, pp. 1–13.

[9]Hauenstein, A. J., Laurenson, R. M., Eversman, W., Galecki, G., Qumei, I., and Amos, A. K., "Chaotic Response of Aerosurfaces with Structural Nonlinearities," *Proceedings of the AIAA/ASME/ASCE/AHS/ASC 31st Structures, Structural Dynamics, and Materials Conference* (Long Beach, CA), AIAA, Washington, DC, 1990, pp. 1530–1539.

[10]Hauenstein, A., Zara, J., Eversman, W., and Qumei, I., "Chaotic and Nonlinear Dynamic Response of Aerosurfaces with Structural Nonlinearities," *Proceedings of the AIAA/ASME/ASCE/AHS/ASC 33rd Structures, Structural Dynamics, and Materials Conference, Part 4 Structural Dynamics II* (Dallas, TX), AIAA, Washington, DC, 1992, pp. 2367–2375.

[11]Tang, D. M., and Dowell, E. H., "Flutter and Stall Response of a Helicopter Blade with Structural Nonlinearity," *Journal of Aircraft*, Vol. 29, No. 5, 1992, pp. 953–960.

[12]Tran, C. T., and Petot, D., "Semi-Empirical Model for the Dynamic Stall of Airfoils in View of the Application to the Calculation of Responses of a Helicopter Blade in Forward Flight," *Vertica*, Vol. 5, No. 1, 1981, pp. 35–53.

[13]Lee, B. H. K., and Desrochers, J., "Flutter Analysis of a Two-Dimensional Airfoil Containing Structural Nonlinearities," National Research Council of Canada, Aeronautical Rept. LR-618, Ottawa, Canada, May 1987.

[14]Fung, Y. C., *An Introduction to the Theory of Aeroelasticity*, Wiley, New York, 1955.

[15]Houbolt, J. C., "A Recurrence Matrix Solution for the Dynamic Response of Elastic Aircraft," *Journal of Aeronautical Sciences*, Vol. 17, Sept. 1950, pp. 540–550.

[16]Jones, D. J., and Lee, B. H. K., "Time Marching Numerical Solutions of the Dynamic Response of Nonlinear Systems," National Research Council of Canada Rept. NAE-AN-25, Ottawa, Canada, Jan. 1985.

[17]Thompson, J. M. T., and Stewart, H. B., *Nonlinear Dynamics and Chaos*, Wiley, Chichester, England, UK, 1986.

[18]Price, S. J., Alighanbari, H., and Lee, B. H. K., "The Aeroelastic Response of a Two-Dimensional Airfoil with Bilinear and Cubic Structural Nonlinearities," *Proceedings of the AIAA/ASME/ASCE/AHS/ASC 35th Structures, Structural Dynamics, and Materials Conference* (Hilton Head, SC), AIAA, Washington, DC, 1994, pp. 1771–1780.